2017 IEEE International Conference on Advanced Intelligent Mechatronics (AIM)
Sheraton Arabella Park Hotel, Munich, Germany, July 3-7, 2017

Positioning of Drug Carriers using Permanent Magnet-Based Robotic System in Three-Dimensional Space

Islam S. M. Khalil*, Abdelrahman Alfar*, Ahmet Fatih Tabak†,
Anke Klingner*, Stefano Stramigioli‡, and Metin Sitti†

***Abstract*— Magnetic control of drug carriers using systems with open-configurations is essential to enable scaling to the size of *in vivo* applications. In this study, we demonstrate motion control of paramagnetic microparticles in a low Reynolds number fluid, using a permanent magnet-based robotic system with an open-configuration. The microparticles are controlled in three-dimensional (3D) space using a cylindrical NdFeB magnet that is fixed to the end-effector of a robotic arm. We develop a kinematic map between the position of the microparticles and the configuration of the robotic arm, and use this map as a basis of a closed-loop control system based on the position of the microparticles. Our experimental results show the ability of the robot configuration to control the exerted field gradient on the dipole of the microparticles, and achieve positioning in 3D space with maximum error of 300 μm and 600 μm in the steady-state during setpoint and trajectory tracking, respectively.**

I. Introduction

Electromagnetic systems with closed-configurations [1], [2] are generally thought to be essential for diverse biomedical applications during *in vitro* experimentation [3], [4], [5], [6]. Due to several technological barriers, these systems cannot be scaled up to the size of *in vivo* applications as it is generally not viable to achieve relatively high gradients at a distance. The limited projection distance of the magnetic field gradient constrains the workspace of these systems to tens of millimeters at most. It is also difficult to integrate a clinical imaging modality to electromagnetic systems with closed-configuration, for instance. These challenges have been partially overcome by Mahoney *et al.* [7], [8]. A combination of magnetic field-driven helical microrobots [9], [10] and a robotic arm with a fixed permanent magnet to its end-effector has been proposed, and used to achieve locomotion throughout relatively large workspace in three-dimensional (3D) space. The rotating dipole field enables the microrobot to achieve helical propulsion, while the robotic arm allows the rotating permanent magnet to generate the rotating fields at any point within its workspace. Recently, Nelson *et al.* [11] have utilized the non-uniformity of the rotating field in generating two independent rotating magnetic fields using a single magnet dipole. Mahoney and Abbott have also demonstrated three degrees-of-freedom (DOFs) position and two DOFs orientation control of a magnetic capsule (a 24-mm-long capsule-shaped untethered magnetic device) using a single permanent magnet positioned via a serial-link manipulator [12]. An open configuration of two synchronized rotating dipole fields has been also introduced in [13], [14] to control the motion of helical microrobot inside catheter segment and in 3D space. The open configuration of this magnetic-based robotic system enables scaling to the size of *in vivo* applications, and its ability to remove blood clots has been demonstrated. An electromagnetic coil and a permanent magnet have been integrated to the end-effector of a robotic arm with 4 DOFs in [15], and a comparative study has shown the ability of the coil to achieve higher positioning accuracy of microparticles compared to the permanent magnet. Although electromagnetic coils provide greater positioning accuracy owing to their ability to control the magnitude of the field gradient via the current input, it is desirable to benefit from the higher magnetic field and field gradient that can be generated using permanent magnets. In this work, we

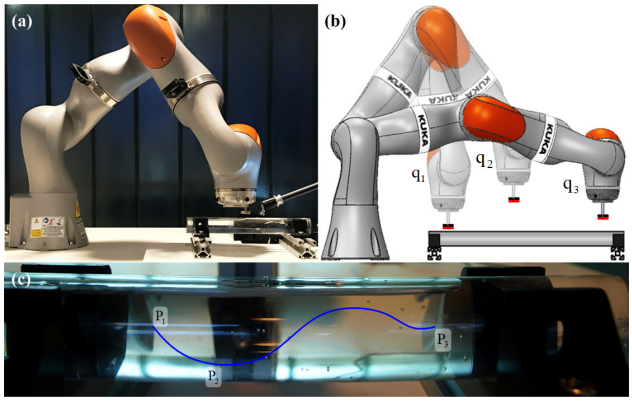

Fig. 1. A permanent magnet-based actuation system is used to control and position paramagnetic microparticles in a low Reynolds number fluid. (a) The system consist of a robotic arm and a cylindrical NdFeB magnet attached to its end-effector. Paramagnetic microparticles with average diameter of 100 μm are contained inside a glass tube and positioned in three-dimensional (3D) space using the field gradients. (b) The configuration of the robotic arm (indicated using the joint space coordinates $\mathbf{q}$) solely control the position of the microparticles in 3D space. (c) The microparticle follows a path (blue trajectory) controllably based on the configuration of the robotic arm. $\mathbf{p}_1$, $\mathbf{p}_2$, and $\mathbf{p}_3$ are the position vectors of the microparticles corresponding to the robotic configurations $\mathbf{q}_1$, $\mathbf{q}_2$, and $\mathbf{q}_3$, respectively.

This work was supported by the Science and Technology Development Fund in Egypt (No. 23016) and the DAAD-BMBF funding project.

*I. S. M. Khalil, A. Alfar, and A. Klingner are with the Department of Mechatronics, The German University in Cairo, New Cairo City, Egypt.

‡S. Stramigioli is with MIRA–Institute for Biomedical Technology and Technical Medicine, University of Twente, Enschede, The Netherlands.

†A. F. Tabak and Metin Sitti are with the Physical Intelligence Department, Max Planck Institute for Intelligent Systems, Stuttgart, Germany.

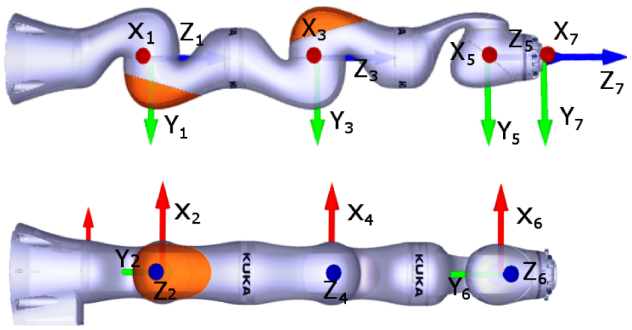

Fig. 2. Frames assignment of the KUKA LBR iiwa 7 R800 robotic arm. A permanent magnet is attached to the end-effector and its magnetization vector and $\mathbf{z}_7$ are collinear.

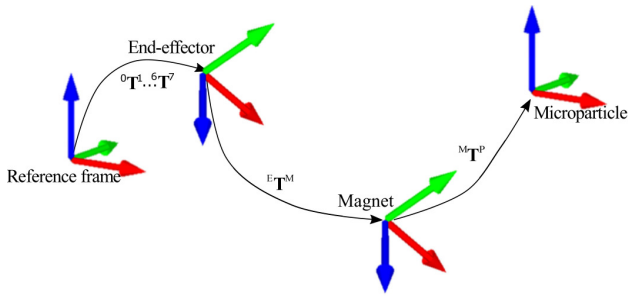

Fig. 3. Position of the microparticles is mapped onto the configuration of the robotic arm using three homogenous transformations. The pose of the end-effector is determined with respect to a frame of reference using $^{0}\mathbf{T}^{7}$. Position of the permanent magnet with respect to the end-effector is defined using $^{7}\mathbf{T}^{\mathrm{M}}$. Position of the microparticle with respect to the magnet is defined using $^{\mathrm{M}}\mathbf{T}^{\mathrm{P}}$.

design a closed-loop control system to position clusters of paramagnetic microparticles (less than 100 μm in diameter) in low Reynolds number fluids. The control is achieved in 3D space using a robotic arm with seven DOFs and a permanent magnet, as shown in Fig. 1. First, we derive a mapping between the position of the cluster of microparticles and the configuration of the robotic arm. This mapping is used a basis of a closed-loop control system to position the cluster in 3D space. Second, we achieve setpoint tracking and trajectory tracking of the microparticles.

The reminder of this paper is organized as follows: Section II provides the kinematic model of the robotic arm and the microparticles, and the closed-loop control system design. Descriptions of the experimental setup and the motion control trials are provided in Section III. Finally, Section IV concludes and provides directions for future work.

II. Kinematic Modeling of the Robotic Arm and Microparticle

Our permanent magnet-based robotic system consists of a robotic arm and a permanent magnet attached to its end-effector. Location and orientation of the permanent magnet are controlled to position the microparticles in 3D space. A magnetic force ($\mathbf{F}(\mathbf{p}) \in \mathbb{R}^{3\times1}$) is exerted on the dipole moment ($\mathbf{m} \in \mathbb{R}^{3\times1}$) of a paramagnetic microparticle, and enables pulling of this microparticle in 3D space (Fig. 1). The magnetic force is generated using a cylindrical NdFeB magnet with a magnetization vector ($\mathbf{M}$) oriented along $\mathbf{y}_7$, as shown in Fig. 2. The permanent magnet is attached to the end-effector of a robotic arm (KUKA LBR iiwa 7 R800) with seven rotational DOFs. Therefore, the magnetic force exerted on the magnetic dipole moment of the microparticle is controlled using the orientation of the permanent magnet and the end-effector of the robotic arm. The Denavit-Hartenberg (DH) frames are shown in Fig. 2. The relation between the frame of reference of the robotic arm and a frame of reference of a microparticle is given by

$$^{0}\mathbf{T}^{\mathrm{P}}(\mathbf{q},\mathbf{p}) = {}^{0}\mathbf{T}^{7}(\mathbf{q})\ {}^{7}\mathbf{T}^{\mathrm{M}}\ {}^{\mathrm{M}}\mathbf{T}^{\mathrm{P}}(\mathbf{p}), \tag{1}$$

where $^{0}\mathbf{T}^{\mathrm{P}}(\mathbf{q},\mathbf{p}) \in \mathbb{R}^{4\times4}$ is the homogenous transformation between the frame of reference of the robotic arm and the frame of reference of the microparticle (Fig. 3). This transformation depends on the generalized coordinates of the robotic arm ($\mathbf{q} \in \mathbb{R}^{7\times1}$) and the position of the microparticle ($\mathbf{p} \in \mathbb{R}^{3\times1}$). Further, $^{0}\mathbf{T}^{7}$ represents the relation between the frame of reference of the robotic arm and the end-effector, and is governed by

$$^{i-1}\mathbf{T}^{i} = \begin{bmatrix} c\theta_i & -s\theta_i & 0 & a_{i-1} \\ s\theta_i c\alpha_{i-1} & c\theta_i c\alpha_{i-1} & -s\alpha_{i-1} & -s\alpha_{i-1}d_i \\ s\theta_i s\alpha_{i-1} & c\theta_i s\alpha_{i-1} & c\alpha_{i-1} & c\alpha_{i-1}d_i \\ 0 & 0 & 0 & 1 \end{bmatrix}, \tag{2}$$

where $^{i-1}\mathbf{T}^{i}$ represents the relation between the $i-1$ frame and i frame of reference ($^{0}\mathbf{T}^{7} = {}^{0}\mathbf{T}^{1}\ldots{}^{6}\mathbf{T}^{7}$). Further, c and s indicate the cosine and sine functions, respectively. Furthermore, α_{i-1}, a_{i-1}, d_i, and θ_i are the DH parameters of the ith frame of reference, and are provided in Table I. In (1), $^{7}\mathbf{T}^{\mathrm{M}}$ represents the relation between the end-effector and the permanent magnet as follows:

$$^{7}\mathbf{T}^{\mathrm{M}} = \begin{bmatrix} 1 & 0 & 0 & 0 \\ 0 & 1 & 0 & 0 \\ 0 & 0 & 1 & l_{\mathrm{M}} \\ 0 & 0 & 0 & 1 \end{bmatrix}, \tag{3}$$

where l_{M} is the length of an adapter used to connect the permanent magnet to the end-effector. Finally, $^{\mathrm{M}}\mathbf{T}^{\mathrm{P}}(\mathbf{p})$

TABLE I
Denavit-Hartenberg (DH) parameters of the KUKA LBR iiwa 7 R800 robotic arm.

i	α_{i-1}	a_{i-1}	d_i	θ_i	i	α_{i-1}	a_{i-1}	d_i	θ_i
1	90	0	0.187	q_1	2	90	0	0	q_2
3	90	0	0.4	q_3	4	90	0.0	0	q_4
5	-90	0.043	0.4	q_5	6	-90	0.043	0	q_6

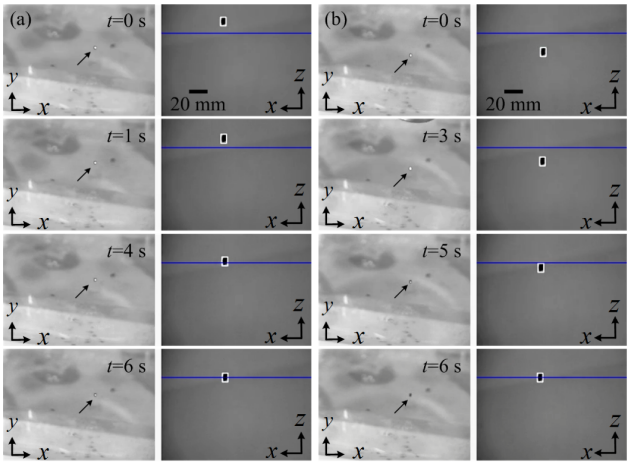

Fig. 4. Representative motion control of a cluster of paramagnetic microparticles using a permanent magnet attached to the robotic arm. The black arrow indicates the position of the cluster in the xy-plane, whereas the blue line represents the reference position along z-axis. (a) A cluster of microparticle is controlled to move downward towards a reference position under the influence of controlled field gradient and its own weight. The field gradient is controlled via the configuration of the robotic arm. (b) The cluster is pulled up towards the reference position using the field gradient.

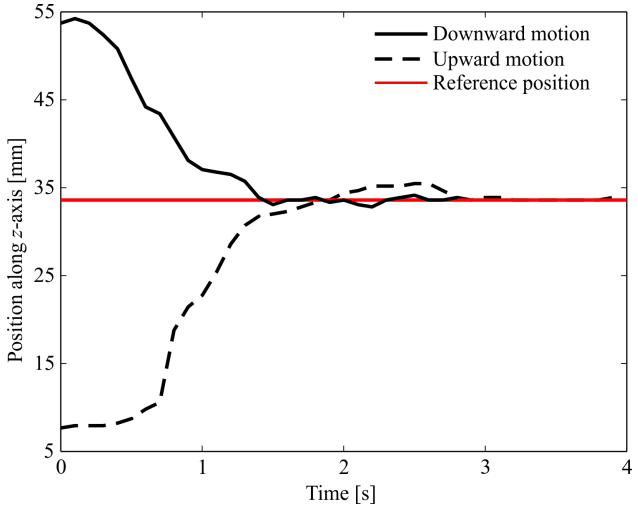

Fig. 5. Representative motion control of a cluster of paramagnetic microparticles using a permanent magnet attached to the end-effector of the robotic arm. The microparticles is controlled to move downward at an average speed of 5.8 mm/s, and is pulled upwards at speed of 7.1 mm/s.

describes the relation between the permanent magnet and the frame of reference of the microparticle. The magnetization of the permanent magnet generates the following magnetic field at the position ($\mathbf{p}$) of the microparticle [16]:

$$\mathbf{B}(\mathbf{p}) = \frac{\mu_0}{4\pi\|\mathbf{x}-\mathbf{p}\|^3}\left(\frac{3\left(\mathbf{M}\cdot(\mathbf{x}-\mathbf{p})\right)(\mathbf{x}-\mathbf{p})}{\|\left(\mathbf{x}-\mathbf{p}\right)\|^2} - \mathbf{M}\right). \tag{4}$$

In (4), $\mathbf{B}(\mathbf{p}) \in \mathbb{R}^{3\times1}$ is the magnetic field on point $\mathbf{p} \in \mathbb{R}^{3\times1}$ and μ_0 is the permeability of free space ($4\pi \times 10^{-7}$ T.m.A^{-1}). $\mathbf{x}$ is the position of the permanent magnet that is attached to the end-effector of the robotic arm. The microparticles we consider are spherical and have no shape anisotropy. Therefore, the microparticles are subjected to pure magnetic force given by

$$\frac{\partial}{\partial i}\left(\mathbf{m}(\mathbf{p})\cdot\mathbf{B}(\mathbf{p})\right) = f_i(\mathbf{p}) \quad \text{for} \quad i = x, y, z, \tag{5}$$

where $\mathbf{m}(\mathbf{p}) \in \mathbb{R}^{3\times1}$ is the magnetic dipole moment of the microparticle and $f_i(\mathbf{P})$ is the ith magnetic force component for $i = x, y, z$. In (5), the magnetic dipole moment of the microparticle is calculated using

$$\mathbf{m}(\mathbf{p}) = \frac{1}{\mu}\frac{4}{3}\pi r_{\mathrm{p}}^3 \chi_{\mathrm{m}}\mathbf{B}(\mathbf{p}), \tag{6}$$

where μ is the permeability coefficient given by, $\mu = \mu_0(1+\chi_{\mathrm{m}})$. Further, χ_{m} is the magnetic susceptibility constant [17] and r_{p} is the radius of the microparticle. The microparticles we use have an average diameter of 100 μm, and are pulled at a maximum speed of 200 μm/s (speed of a single microparticle). At this speed the Reynolds number is calculated as $Re = \frac{\rho_{\mathrm{f}}|\dot{\mathbf{p}}|D}{\eta} = 0.025$, where ρ_{f} is the density of the fluid (1260 kg.m^{-3}), $\dot{\mathbf{p}}$ is the velocity of the microparticle and D is its diameter, and η is the dynamic viscosity of the fluid (10^{-3} Pa.s). Therefore, motion of the microparticle is governed by magnetic, drag, and buoyancy forces as follows:

$$\frac{\partial}{\partial i}\left(\mathbf{m}(\mathbf{p})\cdot\mathbf{B}(\mathbf{p})\right) + 6\pi\eta r_{\mathrm{p}}\dot{\mathbf{p}} + \mathbf{F}_{\mathrm{b}} = 0 \quad \text{for} \quad i = x, y, z, \tag{7}$$

where r_{p} is the radius of the microparticle and $\mathbf{F}_{\mathrm{b}} \in \mathbb{R}^{3\times1}$ is the net buoyancy force (effective gravitational force) and is given by

$$\mathbf{F}_{\mathrm{b}} = V(\rho_{\mathrm{p}} - \rho_{\mathrm{f}})\mathbf{g}. \tag{8}$$

In (8), V is the volume of the microparticle and ρ_{p} is its density. Further, $\mathbf{g}$ is the acceleration vector due to gravity. Setting the magnetic field gradient ($\nabla\left(\mathbf{m}(\mathbf{p})\cdot\mathbf{B}(\mathbf{p})\right)$) to $\mathbf{K}_{\mathrm{p}}\mathbf{e} + \mathbf{K}_{\mathrm{d}}\dot{\mathbf{e}} - \widehat{\mathbf{F}}_{\mathrm{b}}$, where $\widehat{\mathbf{F}}_{\mathrm{b}}$ is the nominal buoyancy force, yields the following error dynamics:

$$\mathbf{K}_{\mathrm{p}}\mathbf{e} + \mathbf{K}_{\mathrm{d}}\dot{\mathbf{e}} + 6\pi\eta r_{\mathrm{p}}\dot{\mathbf{e}} = 0, \tag{9}$$

where $\mathbf{K}_{\mathrm{p}} \in \mathbb{R}^{3\times3}$ and $\mathbf{K}_{\mathrm{d}} \in \mathbb{R}^{3\times3}$ are proportional and derivative positive-definite matrices, respectively. Further, $\mathbf{e} \in \mathbb{R}^{3\times1}$ and $\dot{\mathbf{e}} \in \mathbb{R}^{3\times1}$ are the position and velocity tracking errors, respectively, and $\mathbf{e}$ is given by

$$\mathbf{e} = \mathbf{p} - \mathbf{p}^{\mathrm{r}} = \begin{bmatrix} p_x & p_y & p_z \end{bmatrix}^{\mathrm{T}} - \begin{bmatrix} p_x^{\mathrm{r}} & p_y^{r} & p_z^{\mathrm{r}} \end{bmatrix}^{\mathrm{T}}, \tag{10}$$

where $\mathbf{p}^{\mathrm{r}}$ is a fixed reference position ($\dot{\mathbf{e}} = \dot{\mathbf{p}}$), and p_x^{r}, p_y^{r}, and p_z^{r} are its components along x-, y-, and z-axis, respectively. Implementation of this control system is based on the error dynamics of the microparticle (9). First, we select positive-definite control gains $\mathbf{K}_{\mathrm{p}}$ and $\mathbf{K}_{\mathrm{d}}$, and solve for the desired magnetic forces by setting

$$\mathbf{K}_{\mathrm{p}}\mathbf{e} + \mathbf{K}_{\mathrm{d}}\dot{\mathbf{e}} - \widehat{\mathbf{F}}_{\mathrm{b}} \Rightarrow \nabla\left(\mathbf{m}(\mathbf{p})\cdot\mathbf{B}(\mathbf{p})\right). \tag{11}$$

Using (11), we calculate the magnetic field $\mathbf{B}(\mathbf{p})$. This field is substituted in (4) to calculate the desired position

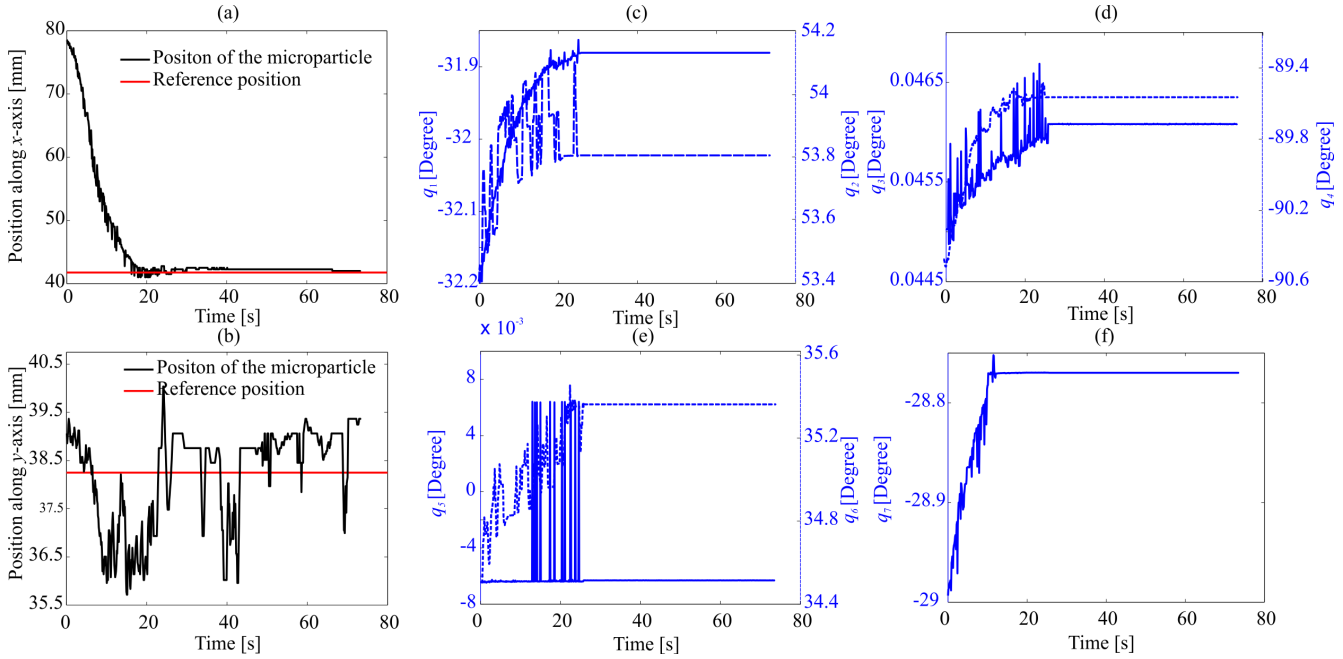

Fig. 6. Kinematic control of a cluster of paramagnetic microparticles is achieved using a permanent magnet attached to the end-effector of the robotic arm. (a) Position of the microparticles along x-axis. The microparticles move at average speed of 1.65 mm/s along x-axis. (b) Motion of the microparticles along y-axis towards the reference position at an average speed of 0.25 mm/s. (c, d, e, and f) Configuration of the robotic arm during the motion control of the microparticles is represented using q_j, for $j = 1, \ldots, 7$.

of the permanent magnet ($\mathbf{x}$). Finally, $\mathbf{x}$ is used to determine the configuration of the robotic arm ($\mathbf{q}$) using its inverse-kinematics. Equations (1), (4), (10), and (11) enable the permanent magnet-based robotic system to control the motion of the microparticles via the configuration of the robotic arm. The first two terms in (11) represent corrective control input, whereas the third term is an equivalent control input. This equivalent control input depends on the densities of the medium and the microparticles, and the volume of the microparticles that can be determined before each trail. Therefore, the equivalent control input is relatively accurate and results in stable linear error dynamics (9).

III. EXPERIMENTAL RESULTS

Motion control trials are done using our permanent magnet-based robotic system (Fig. 1). This system consists of a robotic arm (KUKA iiwa 7 R800, KUKA Robot Automation, Augsburg, Germany). The end-effector of the robot can be controlled at accuracy of ± 0.1 mm. We attach a cylindrical NdFeB magnet (RL21, IBS Magnet, Berlin, Germany) with diameter and hight of 20 mm and 4.3 mm, respectively. The magnetization vector of the cylindrical magnet is oriented along $\mathbf{y}_7$ of the end-effector and generates 400 mT on its surface. The end-effector approaches a reservoir that contains a medium (density of 0.857 g/ml) and paramagnetic microparticles (PLAParticles-M-redF-plain from Micromod Partikeltechnologie GmbH, Rostock-Warnemuende, Germany) with average diameter of 100 μm. The microparticle has magnetization of 4.3 A.m^2/kg and saturation magnetization in excess of 6.6 A.m^2/kg. Position of the microparticles is observed using 2 cameras. Position of the microparticle along xz-plane is determined using a Venus USB2.0 Camera, whereas the position along xy-plane is observed using a monochrome zoom camera (DMK Z12GP031, GigE monochrome zoom camera, The Imaging Source Europe GmbH, Bremen, Germany). A feature tracking algorithm is used to determine the position ($\mathbf{p}$) of the microparticles simultaneously from the xy- and xz views to calculate the position tracking error (10).

First we test the ability of the permanent magnet-based robotic system to suspend the microparticles. Fig. 4 shows two representative trials for controlled microparticles moving towards similar reference position along z-axis. Fig. 4(a) shows a cluster of microparticles moving under the influence of its own weight and controlled magnetic field gradient. The gradient is controlled via the configuration of the robotic arm and at time, t=1.4 seconds, the cluster is positioned at the reference position. Similarly, Fig. 4(b) shows the ability of the system to pull the same cluster upwards towards the reference position and at time, t=1.8 seconds, the cluster is positioned at the reference position. Fig. 5 shows the rise time of the cluster during their motion downward and upward towards the reference position. As one would expect, the rise time of the upward motion is greater than that of the downward motion, as the magnetic force has to overcome the weight while moving upward.

Now we turn our attention to the motion control in 3D space. We provide a reference position to (10) regardless to the initial position of the cluster. Position of the cluster is

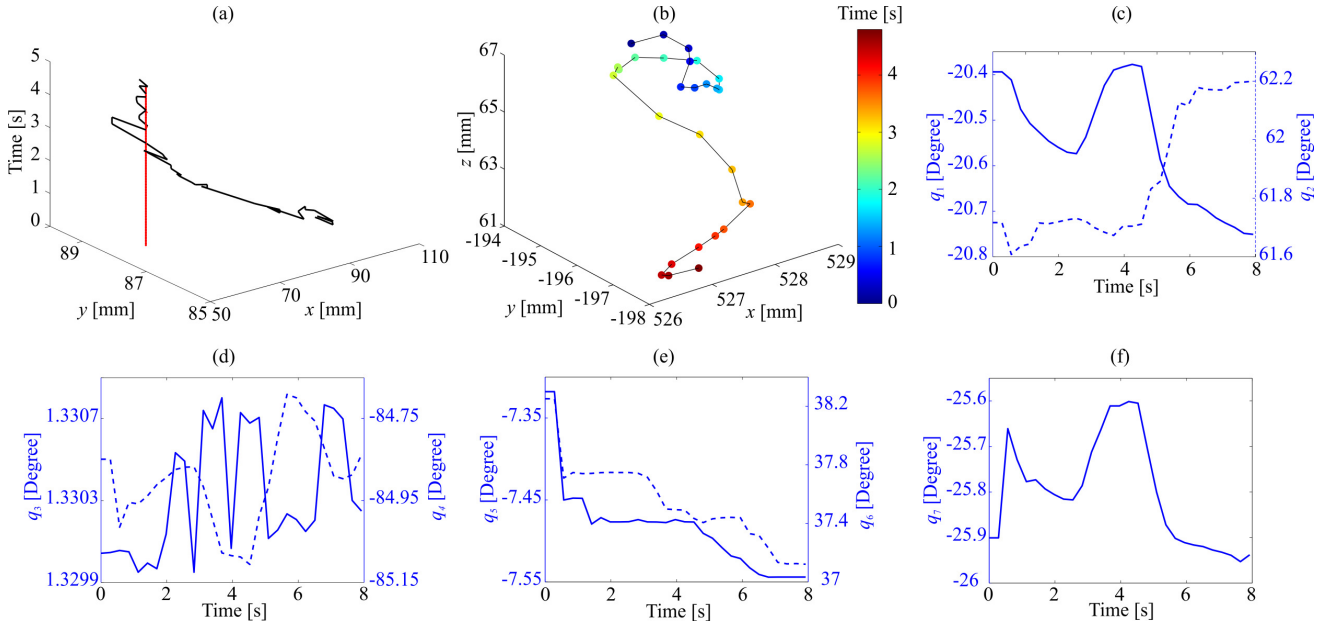

Fig. 7. Kinematic control of a paramagnetic microparticle is achieved using a permanent magnet attached to the end-effector of the robotic arm. (a) A cluster of paramagnetic microparticles is controlled in three-dimensional space towards a reference position (vertical red line). The cluster is pulled towards the reference position at an average speed of 14.3 mm/s and 0.28 mm/s along x- and y-axis, respectively. (b) Position of the end-effector of the robotic arm is calculated during the closed-loop control of the microparticles. (c, d, e, and f) Configuration of the robotic arm during the control of the microparticle.

determined using a feature tracking algorithm in the xy-plane and xz-plane simultaneously. Fig. 6 shows a representative closed-loop control result in 3D space. The microparticles are pulled towards the reference position after 17 seconds. Figs. 6(a) and (b) provide the position of the microparticles along x- and y-axis towards the reference position (horizontal red line), respectively. The configuration of the robotic arm during this closed-loop control trial is shown in Figs. 6(c, d, e, and f) by the generalized coordinates q_j, for $j = 1, \ldots, 7$. In this trial, the microparticles are pulled towards the reference position at an average speed of 1.65 mm/s, and the maximum steady-state error is 200 μm. Another setpoint tracking control result is shown in Fig. 7. The cluster is pulled towards the reference position (vertical red line) at an average speed of 14.3 μm/s, as shown in Fig. 7(a). The maximum position error of the microparticles is 250 μm in the steady-state. Position of the end-effector (and the permanent magnet) is shown in Fig. 7(b), and indicates that the robotic arm positions the microparticles in approximately 4.7 seconds. The configuration of the robotic arm during this representative motion control trial is represented using Figs. 7(c, d, e, and f).

We also examine the ability of the control system to follow a trajectory as shown in Fig. 8. Two reference trajectories (straight line and a sinusoidal trajectory) are divided into waypoints that are shown by the red circles. This experiment shows the ability of the permanent magnet-based robotic system to navigate the microparticles controllably throughout relatively large distance of approximately 500 body-length. The maximum error is calculated to be 600 μm and 300 μm for the straight line and sinusoidal trajectories, respectively.

Despite the nonlinearity of the applied magnetic field (4) and field gradient (5), our control algorithm achieves stable positioning of the microparticles during setpoint and trajectory tracking based on (9). The control law depends on corrective (based on the position and velocity errors) and equivalent (based on the nominal model of the microparticle) inputs. The equivalent control inputs enable us to realize linear error dynamics of the controlled microparticle. However, its effectiveness is limited by the accuracy of the nominal model of the microparticle and the ability to map the desired magnetic force into magnetic field gradients using (11) and (4). We do not also account for the microparticle-to-microparticle interactions during the motion control of a cluster of microparticles. However, Fig. 4 and Fig. 5 demonstrate experimentally the ability of the control system to compensate for the deviations between the equivalent control input and the actual model of the cluster.

IV. CONCLUSIONS AND FUTURE WORK

We demonstrate the ability of permanent magnet-based robotic system to control the motion of paramagnetic microparticles in 3D space. The microparticles are pulled controllably towards the reference position under the influence of magnetic field gradients that are solely controlled via the configuration of the robotic arm. Our experimental results show the ability of the system to position microparticles in 3D space with maximum position error of 300 μm in the steady-state during setpoint tracking and 600 μm during trajectory tracking.

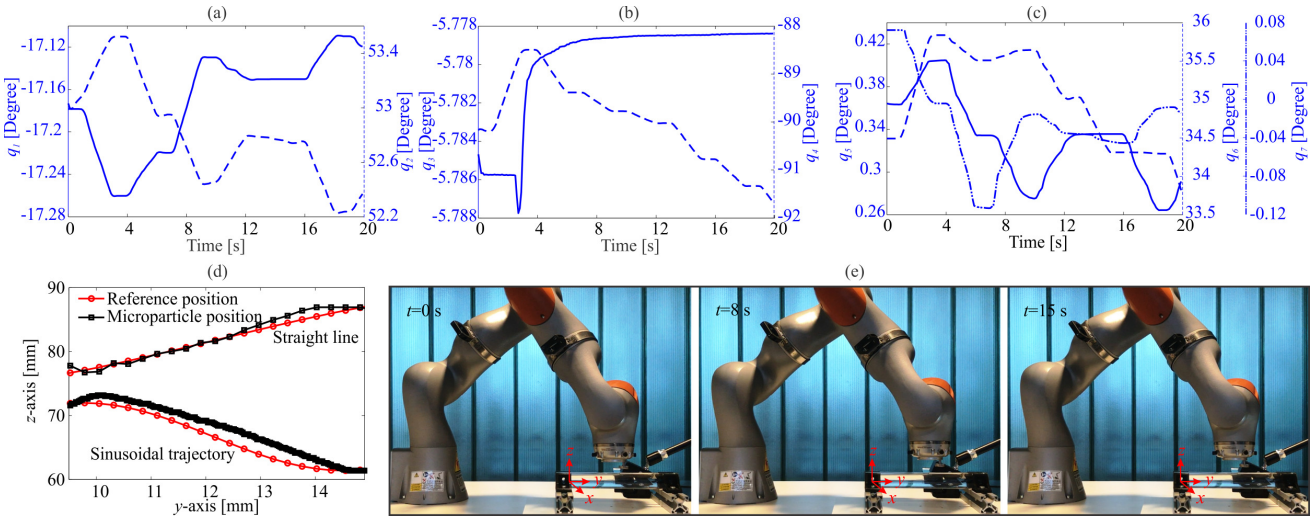

Fig. 8. Straight line and sinusoidal trajectory tracking by the controlled microparticles via the controlled field gradient. (a, b, and c) The configuration of the robotic arm during trajectory tracking of a sinusoidal reference trajectory is represented using q_j, for $j = 1, \ldots, 7$. (d) Waypoints (small red circles) are defined along the reference trajectory (red lines) and control law (11) is implemented based on (10). (e) Representative configurations for the robotic arm during tracking of a sinusoidal trajectory.

As part of future studies, our permanent magnet-based robotic system will be integrated to an ultrasound system to provide feedback instead of the visual feedback provided by the cameras [18]. This modification will enable us to visualize and control the motion of drug carriers such as paramagnetic microparticles and iron-oxide nanoparticles *in vivo*.

REFERENCES

[1] M. P. Kummer, J. J. Abbott, B. E. Kartochvil, R. Borer, A. Sengul, and B. J. Nelson, "OctoMag: an electromagnetic system for 5-DOF wireless micromanipulation," *IEEE Transactions on Robotics*, vol. 26, no. 6, pp. 1006-1017, December 2010.

[2] C. Pawashe, S. Floyd, E. Diller, and M. Sitti, "Two-dimensional autonomous microparticle manipulation strategies for magnetic microrobots in fluidic environments," *IEEE Transactions on Robotics*, vol. 28, no. 2, pp. 467-477, April 2012.

[3] B. J. Nelson, I. K. Kaliakatsos, and J. J. Abbott, "Microrobots for minimally invasive medicine," *Annual Review of Biomedical Engineering*, vol. 12, pp. 55-85, April 2010.

[4] M. Sitti, H. Ceylan, W. Hu, J. Giltinan, M. Turan, S. Yim, and E. Diller, "Biomedical applications of untethered mobile milli/microrobots," *Proceedings of the IEEE*, vol. 103, no. 2, pp. 205-224, February 2015.

[5] J. Wang and W. Gao, "Nano/Microscale motors: biomedical opportunities and challenges," *ACS Nano*, vol. 6, no. 7, pp. 5745-5751, July 2012.

[6] H. Abbass, M. S. Shoukry, S. Misra, and I. S. M. Khalil, "Robust motion control of paramagnetic micro-particles against time-varying flow rates", in *Proceedings of the IEEE RAS/EMBS International Conference on Biomedical Robotics and Biomechatronics (BioRob)*, pp. 67-72, Singapore, June 2016.

[7] A. W. Mahoney, D. L. Cowan, K. M. Miller, and J. J. Abbott, "Control of untethered magnetically actuated tools using a rotating permanent magnet in any position," in *Proceedings of the IEEE International Conference on Robotics and Automation (ICRA)*, pp. 3375-3380, Minnesota, USA, May 2012.

[8] A. W. Mahoney and J. J. Abbott, "Control of untethered magnetically actuated tools with localization uncertainty using a rotating permanent magnet," in *Proceedings of the IEEE RAS/EMBS International Conference on Biomedical Robotics and Biomechatronics (BioRob)*, pp. 1632-1637, Rome, Italy, June 2012.

[9] K. E. Peyer, L. Zhang, and B. J. Nelson, "Bio-inspired magnetic swimming microrobots for biomedical applications", *Nanoscale*, vol. 5, no. 4, pp. 1259-1272, November 2012.

[10] D. J. Bell, S. Leutenegger, K. M. Hammar, L. X. Dong, and B. J. Nelson, "Flagella-like propulsion for microrobots using a magnetic nanocoil and a rotating electromagnetic field", in *Proceedings of the IEEE International Conference on Robotics and Automation (ICRA)*, pp. 1128-1133, April 2007.

[11] N. D. Nelson and J. J. Abbott, "Generating two independent rotating magnetic fields with a single magnetic dipole for the propulsion of untethered magnetic devices," in *Proceedings of the IEEE International Conference on Robotics and Automation (ICRA)*, pp. 4056–4061, Seattle, Washington, USA, May 2005.

[12] A. W. Mahoney and Jake J. Abbott, "Five-degree-of-freedom manipulation of an untethered magnetic device in fluid using a single permanent magnet with application in stomach capsule endoscopy," *The International Journal of Robotics Research*, vol. 35, no. 1-3, pp. 129–147, February 2016.

[13] A. Hosney, A. Klingner, S. Misra, and I. S. M. Khalil, "Propulsion and steering of helical magnetic microrobots using two synchronized rotating dipole fields in three-dimensional space," in *Proceedings of the IEEE/RSJ International Conference of Robotics and Systems (IROS)*, pp. 1988–1993, Hamburg, Germany, November 2015.

[14] I. S. M. Khalil, A. F. Tabak, K. Sadek, D. Mahdy, N. Hamdi, and M. Sitti, "Rubbing against blood clots using helical robots: modeling and *in vitro* experimental validation, *IEEE Robotics and Automation Letters*, vol. 2, no. 2, pp. 927–934, April 2017.

[15] I. S. M. Khalil, B. E. Wissa, B. G. Salama, and S. Stramigioli, "Wireless motion control of paramagnetic microparticles using a magnetic-based robotic system with an open-configuration," *In Proceedings of the International Conference on Manipulation, Manufacturing and Measurement on the Nanoscale (3M Nano)*, pp. 190-196, Changchun, China, October 2015.

[16] T. W. R. Fountain, P. V. Kailat, and J. J. Abbott, "Wireless control of magnetic helical microrobots using a rotating-permanent-magnet manipulator," in *Proceedings of the IEEE International Conference on Robotics and Automation (ICRA)*, pp. 576–581, Alaska, USA, May 2005.

[17] R. G. McNeil, R. C. Ritter, B. Wang, M. A. Lawson, G. T. Gillies, K. G. Wika, E. G. Quate, M. A. Howard, and M. S. Grady, "Characteristics of an improved magnetic-implant guidance system," *IEEE Transactions on Biomedical Engineering*, vol. 42, no. 8, pp. 802-808, August 1995.

[18] S. Tognarelli, V. Castelli, G. Ciuti, C. Di Natali, E. Sinibaldi, P. Dario, and A. Menciassi, "Magnetic propulsion and ultrasound tracking of endovascular devices" *Journal of Robotic Surgery*, vol. 6, no. 1, pp. 5–12, December 2012.